Journal of Anatolian Environmental and Animal Sciences
(*Anadolu Çevre ve Hayvancılık Bilimleri Dergisi*)
DOI: https://doi.org/10.35229/jaes.681179

JAES
Year: 5, No: 2, 2020 (218-223)
AÇEH
Yıl: 5, Sayı: 2, 2020 (218-223)

ARAŞTIRMA MAKALESİ **RESEARCH PAPER**

Relationship of Urban Development with the Heat Islands, Trabzon Case Study

Burak KAZANCI* **Fulya Başak SARIYILMAZ**
Gumushane University, Faculty of Engineering and Natural Sciences, Department of Geomatics, Gumushane, Turkey

Geliş/Received: *28.01.2020* ***Kabul/Accepted:*** *10.06.2020*

How to cite: **Kazancı, B. & Sarıyılmaz, F.B. (2020).** Relationship Of Urban Development With The Heat Islands, Trabzon Case Study. *J. Anatolian Env. and Anim. Sciences*, *5*(2), 218-223.
Atıf yapmak için: **Kazancı, B. & Sarıyılmaz, F.B. (2020).** Kentsel Gelişmenin Isı Adalarına Etkisinin Araştırılması, Trabzon İli Örneği. *Anadolu Çev. ve Hay. Dergisi*, *5*(2), 218-223.

*: https://orcid.org/0000-0001-8652-7142
: https://orcid.org/0000-0002-4950-3771

***Corresponding author's:**
Burak KAZANCI
Gumushane University, Faculty of Engineering and Natural Sciences, Department of Geomatics, Gumushane, Turkey
✉: burakkazanci61@gmail.com
Mobile telephone : +90 (534) 862 84 28

Abstract: Trabzon, a developing port town province that is located near the Black Sea region of Turkey. Trabzon, the 29th most crowded province of Turkey shows the intensity of urbanization on the coastal zone. In this study, it is aimed to examine the urban development of Trabzon province by using various remote sensing methods and data. Depending on the characteristic of urban development within the boundaries of the province, the change in the artificial surfaces has been investigated by using optical remote sensing methods in the selected test region. For this purpose, LANDSAT images of the study area, 1989, 2000, 2006 and 2018 were provided. Pixel-based supervised classification was applied to the images and the land use and land cover (LULC) classes of the study area were determined. In the second stage of the study, the development of artificial surfaces was investigated by using thermal remote sensing methods. For this purpose, the surface temperature map of the region has been established. By using the thermal bands of the images, top of athmospheric spectral radiance and then brightness temperature were calculated. NDVI, proportion of vegetatiton and ground emissivity were also calculated by using red and near infrared bands. These informations were used in the LST calculation. As a result of the study, the urban development and change taking place in Trabzon by using different remote sensing data and methods were examined.

Keywords: Artificial Surface, Classification, Heat Island.

Kentsel Gelişmenin Isı Adalarına Etkisinin Araştırılması, Trabzon İli Örneği

***Sorumlu yazar:**
Burak KAZANCI
Gümüşhane Üniversitesi, Mühendislik ve Doğa Bilimleri Fakültesi, Geomatik Bölümü, Gümüşhane, Turkey
✉: burakkazanci61@gmail.com
Cep telefonu : +90 (534) 862 84 28

Öz: Trabzon, Türkiye'nin Karadeniz Bölgesi'nde yer alan gelişmekte olan bir liman kentidir. Türkiye'nin en kalabalık 29. vilayeti olan Trabzon'da daha çok kıyı bölgelerde yerleşim mevcuttur. Bu çalışmada Trabzon ilinin kentsel gelişiminin çeşitli uzaktan algılama yöntemleri ve verileri kullanılarak incelenmesi amaçlanmıştır. İlin sınırları içindeki kentsel gelişimin özelliklerine bağlı olarak, seçilen bölgede optik uzaktan algılama yöntemleri kullanılarak yapay yüzeylerdeki değişim araştırılmıştır. Bu amaçla 1989, 2000, 2006 ve 2018 tarihli LANDSAT görüntüleri kullanılmıştır. Görüntülere piksel tabanlı kontrollü sınıflandırma işlemi uygulanmış ve çalışma alanının arazi kullanımı ve arazi örtüsü sınıfları belirlenmiştir. Çalışmanın ikinci aşamasında termal uzaktan algılama yöntemleri kullanılarak yapay yüzeylerin gelişimi araştırılmıştır. Bu amaçla bölgenin yüzey sıcaklık haritası oluşturulmuştur. Görüntülerin termal bantları kullanılarak, atmosfer üstü spektral ışıma ve daha sonra parlaklık sıcaklığı hesaplanmıştır. NDVI değerleri, bitki oranı ve yer emisyonu haritaları da kırmızı ve yakın kızılötesi bantlar kullanılarak hesaplanmıştır. Bu bilgilerin tümü arazi yüzey sıcaklığı haritalarının oluşturulmasında ve kentsel ısı adası etkisinin belirlenmesinde kullanılmıştır. Çalışma sonucunda farklı uzaktan algılama verileri ve yöntemleri kullanılarak Trabzon'da gerçekleşen kentsel gelişim ve değişim incelenmiştir.

Anahtar kelimeler: Yapay yüzeyler, sınıflandırma, ısı adası.

INTRODUCTION

In urban areas, conditions that are of primary importance for human life, such as work, education, health service and residential areas, lead to population growth. With the increasing population, LULC in the cities show a dynamic change. While the areas covered with artificial surfaces increase, the areas covered with vegetation are gradually decreasing. Urban buildings hold a significant amount of solar radiation and affect atmospheric properties in these areas. Urban heat islands (UHIs) are formed in this way. The regions that have higher temperature characteristics than the rural areas in the cities are called as UHI.

More successful and efficient planning is needed to reduce the negative effects of heat islands in urban areas. In order to make these plans, the UHIs should be determined first of all. Remote sensing methods and satellite imagery allow these areas to be identified in less time with less cost. There are many studies examining the relationship between heat islands and LULC using satellite imagery and digital image processing methods (Weng, et al., 2004; Chen, et al., 2006; Zhang, et al., 2009; Jiang, et al., 2010; Li, et al., 2011; Estoque, et al., 2017; Pal, et al., 2017; Yüksek, 2017; Wang, et al., 2018, Du, et al., 2019, Wang, et al., 2019, Sultana and Satyanarayana, 2020). When these studies were examined, it was determined that higher temperatures were calculated in areas covered with artificial surfaces and lower temperatures in areas covered with vegetation and water.

Study Area: Ortahisar District of Trabzon was chosen as the study area. Trabzon is the 29th most populous city of Trabzon (Url-1, 2019). The city is located in the Eastern Black Sea Region of the Black Sea Region. Trabzon and also Ortahisar District have coasts to the Black Sea. After a narrow coastline, the province has an area covered with mountains extending perpendicular to the sea. The temperature in Trabzon varies between 7.4 and 23.5 ˚C throughout the year (Url-1, 2019). Figure 1 shows the study area, Trabzon and Ortahisar District.

Figure 1. The Study area: Trabzon and Ortahisar Distirct.

Ortahisar is the district with the highest population density in Trabzon. Trabzon became a metropolitan municipality with the law adopted on 12 November 2012. The central district was abolished, and Ortahisar District was established by this law (Url-1, 2019). The area of Ortahisar is approximately 235 km^2. The port was built in 1954 and the airport was built in 1957 inside the district (Url-1, 2019).

MATERIAL USED

In order to determine LULC in Ortahisar District and, to obtain the surface temperature map of the study area; LANDSAT 5 TM and LANDSAT 8 OLI images of September 1989, 2000, 2006 and 2018 were used. The satellite images used were provided free of charge from the LANDSAT USGS website and in the UTM WGS 84 coordinate system and datum. Table 1 shows LANDSAT 5 TM and LANDSAT 8 OLI sensor properties (Url-2 2019, Url-3, 2019).

Table 1. LANDSAT 5 TM and LANDSAT 8 OLI sensor features.

Bands	LANDSAT 5	LANDSAT 8
Band 1	30 m Blue	30 m Coastal/Aerosol
Band 2	30 m Green	30 m Blue
Band 3	30 m Red	30 m Green
Band 4	30 m NIR	30 m Red
Band 5	30 m SWIR-1	30 m NIR
Band 6	60 m TIR	30 m SWIR-1
Band 7	30 m SWIR-2	30 m SWIR-2
Band 8	-	15 m PAN
Band 9	-	30 m Cirrus
Band 10	-	100 m TIR-1
Band 11	-	100 m TIR-2

Band 10 of LANDSAT 8 OLI image were used for thermal remote sensing studies, because this band is compatible with the band 6 of LANDSAT 5 TM image.

In addition, the surface temperatures obtained from the meteorological stations were used in order to compare the calculated surface temperatures.

METHOD

In the first stage of the study, artificial surface areas in the region were determined by using optical remote sensing methods. In this study, land cover and land use in Ortahisar District were determined primarily. For this purpose, pixel based classification was performed by using unsupervised and supervised classification algorithm. In the second stage of the study, artificial surface areas in the region were determined by using thermal remote sensing methods. For this purpose, land surface temperatures were determined and mapped by using NDVI thresholding method.

Classification: The overall objective of image classification procedures is to automatically categorize all of the pixels in an image into land cover classes or themes (Lillesand et al., 2004). In this study, pixel based classification method was used for this aim. To obtain LULC classes based on CORINE database level one unsupervised and supervised classification algorithms used together as a hybrid classification.

An accuracy assessment process was performed for each classified images by using error matrix. In order to express the thematic accuracy of the classified image, the overall accuracy and the kappa statistical value was calculated by using random sample points. The binomial sampling method was used to determine the number of samples. The equation used in the binomial sampling method was as follows (VanGenderen et al., 1977; Fitzpatrick, et al, 1981):

$$N = (Z^2pq)/E^2 \quad (1)$$

In this equation; N is the number of samples, p is the expected accuracy, q= 100 – p, E is the error tolerance and Z is the standard normal deviation (For %95 confidence interval, it is equal to 1.96).

Thermal Band Processing: The process steps for determining the land surface temperature (LST) and mapping the urban heat island effect are shown in the Figure 2.

In this study, the TIR band was used to estimate brightness temperature and red band and near infrared (NIR) band were used for calculating the NDVI. The metadata of the satellite images used in the algorithm is presented in Table 2 (Avdan, et al., 2016; Yamak, et al., 2019).

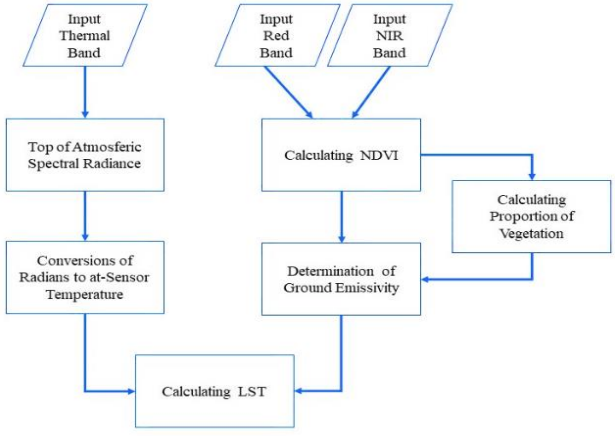

Figure 2. Flowchart for LST.

Table 2. Metadata of LANDSAT Images

Metadata		LANDSAT 5	LANDSAT 8
K_1	Thermal	607,76	774,8853
K_2	Constant	1260,56	1321,0789
M_1	Rescaling	0,055375	0,0003342
A_L	Factor	1,18243	0,1
O_i	Correction	-	0,29

The first step of the process is to calculate the top of atmospheric (TOA) spectral radiance (L_λ) by using the Formula 4 and metadata taken from the USGS web page:

$$L_\lambda = M_L * Q_{cal} + A_L - (O_i) \quad (4)$$

where M_L represents the band-specific multiplicative rescaling factor, Q_{cal} is the thermal infrared (TIR) band of the image, A_L is the band-specific additive rescaling factor, and O_i is the correction for the TIR band of LANDSAT 8 data (Barsi et al., 2014, Avdan, et al., 2016).

After the digital numbers (DNs) of the TIR band are converted to reflection, the data should be converted from spectral radiance to brightness temperature (BT) using the thermal constants provided in the metadata file. The following equation is used to convert reflectance to BT (Avdan, et al., 2016; Yamak, et al., 2019):

$$BT = (K_2/(\ln[(K_1/L_\lambda) + 1])) - 273.15, \quad (5)$$

where K_1 and K_2 stand for the band-specific thermal conversion constants from the metadata.

Normalized Difference Vegetation Index (NDVI) was calculated for all images in the next stage of the study. The calculation of the NDVI is needed because, the proportion of the vegetation (P_V) should be calculated subsequently, and they are highly related with the NDVI results, and then emissivity (ε) was calculated, which is related to the P_V.

NDVI is calculated by using red and NIR bands as shown in the Formula 6 (Ratnayake, 2012):

$$NDVI = (NIR - Red)/(NIR + Red) \quad (6)$$

P_V is also calculated based on NDVI results as shown in the Formula 7 (Wang, et al., 2015; Avdan, et al., 2016):

$$P_V = ((NDVI - NDVI_{min})/(NDVI_{max} - NDVI_{min}))^2 \quad (7)$$

After this stage, in order to calculate the LST, it is necessary to calculate the land surface emission (LSE). Equation used for this purpose is given in Formula 8 (Sobrino, et al., 2004; Avdan et al., 2016):

$$\varepsilon_\lambda = \varepsilon_{V\lambda} P_V + \varepsilon_{S\lambda} (1 - P_V) + C_\lambda, \quad (8)$$

where ε_V and ε_S are the vegetation and soil emissivities, respectively, and C represents the surface roughness (C = 0 for homogenous and flat surfaces) taken as a constant value of 0.005 (Sobrino, et al., 2000; Avdan, et al., 2016).

Formula 9 and Formula 10 were used to calculate LST after calculation LSE (Stathopoulou, et al., 2007; Avdan, et al., 2016).

$$LST = (BT/(1 + ((\lambda BT/\rho) \ln\varepsilon_\lambda)))) \quad (9)$$

where λ is the wavelength of emitted radiance (for which the peak response and the average of the limiting wavelength (λ = 10.895) (Markham, et al., 1985; Avdan et al., 2016) will be used) and

$$\rho = h^* (c/\varphi) = 1.438 \times 10{-}2 \text{ m K}, \quad (10)$$

where φ is the Boltzmann constant (1.38×10^{-23} J/K), *h* is Planck's constant (6.626×10^{-34} Js), and *c* is the velocity of light (2.998×108 m/s) (Barsi, et al, 2014; Avdan et al., 2016).

After the calculation of LST, the urban heat island (UHI) effect was analyzed by using Formula 11:

$$UHI = \mu + (\sigma/2) \quad (11)$$

Where μ is the average LST value of the study area and σ is the standard deviation of the LST (Yamak, et al., 2019).

RESULTS AND CONCLUSION

In this study, unsupervised and supervised classification methods were applied as hybrid classification to all the images to determine the LULC classes. As a result of classification process, four classes based on the first level of CORINE classification system were determined in the study area. These classes are forest and semi-natural areas (FSNA), water bodies (WB), artificial surfaces (AS) and agricultural areas (AA). Figure 3 shows the classification result.

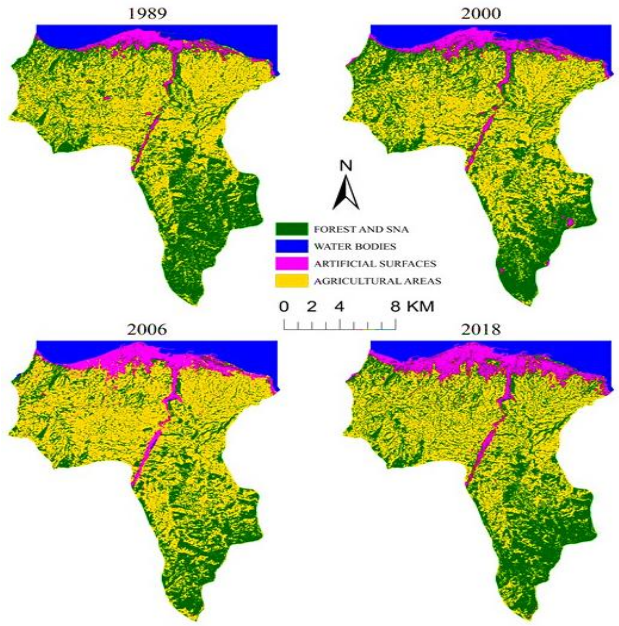

Figure 3. Classified Images.

Accuracy analysis was applied to the images after classification process. As a result of this analysis, overall accuracy and kappa statistical value of all classified images were calculated. Table 4 shows the results of the accuracy analysis.

Table 4. Accuracy analysis results.

Date	Overall Accuracy	Kappa Statistical Value
1989	89%	0.83
2000	84%	0.77
2006	85%	0.78
2018	85%	0.79

As a result of the classification process, it was determined which thematic class covers how much areas of the image. These values are shown in the Table 5.

Table 5. Classification results.

Classes	Years			
	1989	2000	2006	2018
FSNA	43%	42%	33%	43%
WB	11%	11%	10%	10%
AS	4%	5%	8%	9%
AA	42%	42%	49%	38%
TOTAL	100%	100%	100%	100%

When the Table 5 is examined, it is understood that the artificial surface areas within the study area increased by 125% in the period between 1989 and 2018.

In the next stage of the study, the LSTs were calculated for each year by following the process steps. The LST value varied between 12-27 °C in 1989, 8-27 °C in 2000, 11-31 °C in 2006 and 15-28 °C in 2018. Accordingly, the year in which the maximum temperature is highest is 2006 and the year in which the minimum temperature is highest is 2018. Figure 4 shows the LST maps.

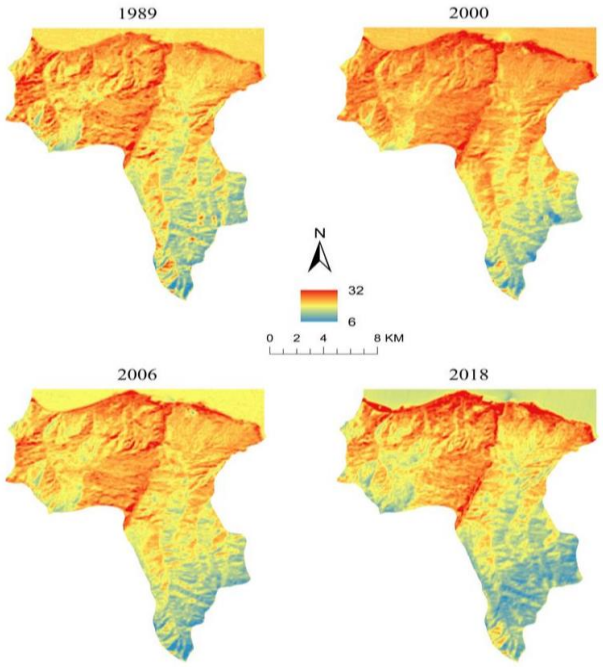

Figure 4. LST Maps.

Table 6. Temperature values.

Station Name	Soil T. (07:00)	Soil T. (Average)	LST
	29.09.1989		
Trabzon	18.2	22.3	21.6
	11.09.2000		
Trabzon	16.9	20.9	20.7
	28.09.2006		
Airport	-	23.7	22.1
	13.09.2018		
Trabzon	20.4	24.5	22.6

In order to compare with the LST values, the temperature values measured at the stations within the

boundaries of the study area were obtained from the Turkish State Meteorological Service. These values are given in Table 6. When Table 6 is examined, it is understood that the calculated values and the measured values are compatible with each other.

UHI effect was calculated in the last stage of the study. According to this, it was determined that UHI was affected by hotter than 19.91 degrees in 1989, 19.81 degrees in 2000, 22.32 degrees in 2006 and 21.37 degrees in 2018. The maps showing the relationship between the artificial surfaces and UHI are given in Figure 5.

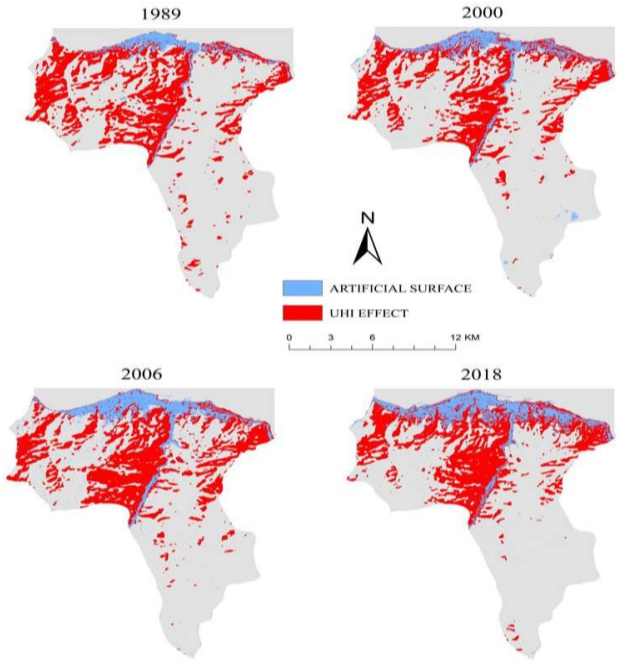

Figure 5. Comparison of UHI with Classification Results.

In this study, it is aimed to reveal the effect of urbanization on LST. For this purpose, LANDSAT images dated 1989, 2000, 2006 and 2018 were used. First of all, the LULC classes in Ortahisar District were determined. Then, LST maps were generated by NDVI thresholding method using thermal, red and NIR bands. Using LST maps, the areas where UHI effect was observed were determined. Accordingly, in the period from 1989 to 2018, it was calculated that there was a 13% increase in the areas where UHI effect was observed. When the images are examined, it is seen that the temperature rises to the highest levels around residential areas, airports, ports and roads. The results obtained with this study can be used to make environmental plans by decision makers.

ACKNOWLEDGEMENTS

This study was presented as an oral presentation at International Symposium on Applied Geoinformatics (ISAG) 2019.

REFERENCES

Avdan, U. & Jovanovska, G. (2016). Algorithm for automated mapping of land surface temperature using LANDSAT 8 satellite data, Journal of Sensors.

Barsi, J. A., Schott, J. R., Hook, S. J., Raqueno, N. G., Markham, B. L. & Radocinski, R. G. (2014). Landsat-8 thermal infrared sensor (TIRS) vicarious radiometric calibration. *Remote Sensing*, ***6***(11), 11607-11626.

Chen, X. L., Zhao, H. M., Li, P. X. & Yin, Z. Y. (2006). Remote sensing image-based analysis of the relationship between urban heat island and land use/cover changes. *Remote Sensing of Environment*, ***104***, 133-146.

Du, H., Ai, J., Cai, Y. & Liu, P. (2019). Combined effects of the surface urban heat island with landscape composition and configuration based on remote sensing: A case study of Shanghai, China. *Sustainability*, ***11***(10), 1-13.

Estoque, R. C., Murayama, Y., & Myint, S. W. (2017). Effects of landscape composition and pattern on land surface temperature: An urban heat island study in the megacities of Southeast Asia. *Science of the Total Environment*, **577**, 349-359.

Fitzpatrick–Lins, K. (1981). Comparison of sampling procedures and data analysis for a land use and land cover map. *Photogrammetric Engineering and Remote Sensing*, ***47***, 343-351.

Jiang, J. & Tian, G. (2010). Analysis of the impact of land use/land cover change on land surface temperature with remote sensing. *Procedia Environmental Sciences*, ***2***, 571-575.

Li, J., Song, C., Cao, L., Zhu, F., Meng, X. & Wu, J. (2011). Impacts of landscape structure on surface urban heat islands: A case study of Shanghai, China. *Remote Sensing of Environment*, 115, 3249-3263.

Lillesand, T.M., Kiefer, R.W. & Chipman, J.W., (2004). *Remote Sensing and Image Interpretation*. 5th Edition, Wiley, USA.

Markham B. L. & Barker, J. L. (1985). Spectral characterization of the Landsat Thematic Mapper sensors. *International Journal of Remote Sensing*, ***6***(5), 697-716.

URL-1. https://tr.wikipedia.org/wiki/Trabzon, 29.09.2019

URL-2. https://www.usgs.gov/media/images/landsat-8-band-designations, 29.09.2019

URL-3. https://www.usgs.gov/faqs/what-are-best-landsat-spectral-bands-use-my-research?qt-news_science_products=0#qt-news_science_products, 29.09.2019

Pal, S. & Ziaul, S. (2017). Detection of land use and land cover change and land surface temperature in English Bazar urban centre. *The Egyptian Journal of Remote Sensing and Space Sciences*, ***20***, 125-145.

Ratnayake, R. (2002). *Forest cover estimation using Normalised Difference Vegetation Index (NDVI) in plantation forest.* Remote Sensing for

Agriculture, Ecosystems, and Hydrology III, Manfred Owe, Guido D'Urso, Editors, Proceedings of SPIE, 4542 SPIE 0277-786X/02.

Sobrino, J.A., Jimenez-Munoz, J.C. and Paolini, L. (2004). Land surface temperature retrieval from LANDSAT TM 5. *Remote Sensing of Environment*, ***90***(4), 434-440.

Sobrino J. A. & Raissouni, N. (2000). Toward remote sensing methods for land cover dynamic monitoring: application to Morocco. *International Journal of Remote Sensing*, ***21***(2), 353-366.

Stathopoulou, M. & Cartalis, C. (2007). Daytime urban heat islands from Landsat ETM+ and Corine land cover data: an application to major cities in Greece. *Solar Energy*, ***81***(3), 358-368.

Sultana, S. & Satyanarayanan, A.N.V. (2020). Assessment of urbanisation and urban heat island intensities using landsatimageries during 2000-2018 over a sub-tropical Indian City. *Sustainable Cities and Society*, ***52***, 1-14. DOI: 10.1016/j.scs.2019.101846

Van Genderen, J.L. & Lock, B.F. (1977). Testing land use map accuracy. *Photogrametric Engineering and Remote Sensing*, ***43***(9), 1135-1137.

Wang, F., Qin, Z., Song, C., Tu, L., Karnieli, A. & Zhao, S. (2015). An improved mono-window algorithm for land surface temperature retrieval from landsat 8 thermal infrared sensor data. *Remote Sensing*, ***7***(4), 4268-4289.

Wang, S., Ma, Q., Ding, H. & Liang, H. (2018). Detection of urban expansion and land surface temperature change using multi-temporal Landsat images. *Resources, Conservation and Recycling*, ***128***, 526–534.

Wang, W., Liu, K., Tang, R. & Wang, S. (2019). Remote sensing image-based analysis of the urban heat island effect in Shenzhen, China. *Physics and Chemistry of the Earth*, ***110***, 168-175.

Weng, Q., Lub, D. & Schubringa, J. (2004). Estimation of land surface temperature–vegetation abundance relationship for urban heat island studies. *Remote Sensing of Environment*, ***89***, 467-

Yamak, B., Yagci, Z., Bilgilioglu, B.B. & Comert, R. (2019). Investigation of the effect of urbanization on land surface temperature: Bursa Case Study, https://www.researchgate.net/publication/333758700, Conference paper, pp. 189-195 (In Turkish).

Yüksek, T . (2017). Land Use, Some Forestry Studies and a General Evaluation of the Temporal Distribution of Precipitation in Rize. *Journal of Anatolian Environmental and Animal Sciences* , ***2***(3), 59-66.

Zhang, X., Zhong, T., Wang, K. & Cheng, Z. (2009). Scaling of impervious surface area and vegetation as indicators to urban land surface temperature using satellite data, *International Journal of Remote Sensing*, ***30***(4), 841-859.